

BAYESRACE: Learning to race autonomously using prior experience

Achin Jain *
Amazon Web Services
achij@amazon.com

Matthew O’Kelly
University of Pennsylvania
mokelly@seas.upenn.edu

Pratik Chaudhari
University of Pennsylvania
pratikac@seas.upenn.edu

Manfred Morari
University of Pennsylvania
morari@seas.upenn.edu

Abstract: Autonomous race cars require perception, estimation, planning, and control modules which work together asynchronously while driving at the limit of a vehicle’s handling capability. A fundamental challenge encountered in designing these software components lies in predicting the vehicle’s future state (*e.g.* position, orientation, and speed) with high accuracy. The root cause is the difficulty in identifying vehicle model parameters that capture the effects of lateral tire slip. We present a model-based planning and control framework for autonomous racing that significantly reduces the effort required in system identification and control design. Our approach alleviates the gap induced by simulation-based controller design by learning from on-board sensor measurements. A major focus of this work is empirical, thus, we demonstrate our contributions by experiments on validated 1:43 and 1:10 scale autonomous racing simulations.

Keywords: Autonomous racing, Gaussian processes, model predictive control, system identification

1 Introduction

Racing drivers first prepare in a simulator before fine-tuning their racing strategy on the real track to compensate for sim-to-real differences. Analogously, in autonomous racing, to optimize the performance of a controller on a real vehicle, we must learn to compensate for the mismatch between the model used in the simulation and real vehicle dynamics. Bridging the simulation-to-reality gap is challenging because it is hard to obtain a high fidelity model of vehicle dynamics, especially at the limit of the vehicle’s handling capability. While the kinematics of the vehicle are precisely known, the dynamics, specifically the lateral tire forces, are complex nonlinear functions whose identification requires multiple time-intensive experiments, see, for example [1]. Using the wrong model parameters severely affects both the controller’s performance and safety. Moreover, since the tire forces strongly depend upon the racing surface, one must repeat the process of system identification if the track or vehicle condition is changed. In this paper, we present a model-based planning and control framework for autonomous racing that significantly reduces the effort required in model identification by learning from prior experience.

Related work. The tasks of autonomous racing and autonomous driving are challenging problems in both the control and reinforcement learning communities with solutions often straddling the two disciplines. In both problem formulations a central characteristic is whether the approach is model-free or model-based. Model-free approaches directly map from vehicle state to actions. For example, Bojarski et al. [2] and Balaji et al. [3] map images from a camera directly to control actions like steering and throttle via a deep neural network. Alternatively, Kapania and Gerdes [4] solve an iterative learning control problem in which the gains of a proportional derivative (PD) controller are tuned to track a racing line as new laps are completed.

*Work done while at University of Pennsylvania

Despite progress in model-free methods, model-based methods like model predictive control (MPC) are more suitable for autonomous racing due to the safety-critical nature of the task and their data efficiency. MPC predicts future vehicle states using a model of the vehicle dynamics and explicitly handles track constraints and obstacle avoidance, allowing the vehicle to execute aggressive maneuvers while staying under control. MPC can be implemented in the form of hierarchical receding horizon control or model predictive contouring control (MPCC)[5]. The performance of MPC is predicated on the correct choice of model parameters. Thus, learning-based control algorithms play an important role in autonomous racing, where we seek to correct the inaccurate parameter estimates by collecting real-world data. In light of this, Rosolia and Borrelli [6] propose an iterative procedure that uses data from previous laps to identify an affine time-varying model of vehicle dynamics and reformulate the MPC problem with an updated terminal set and terminal cost. Similarly, Hewing et al. [7] demonstrate that model mismatch up to $\pm 15\%$ can be fixed with the help of a Gaussian process (GP) model in the MPCC problem. All the above variants of MPC use the *dynamic model*, which is time-intensive to tune; see an in-depth comparison of different types of vehicle models in Section 2. In contrast, Deisenroth and Rasmussen [8] propose learning black-box representations of the system’s dynamics using GPs as well as learning the control policy rather than solving the optimal control (MPC) problem online. Unlike [8], *residual* physics-based methods learn to correct the output of a structured model or controller [9, 10, 11]. Our residual physics-based approach utilizes a simple *extended kinematic model* that has only three easily measurable vehicle parameters. The residual component of the dynamics is captured using GP models.

Contributions. We use the extended kinematic model (all three parameters – mass, the distance of the center of gravity from the front and rear wheels – can be physically measured) as a nominal model. Then using Gaussian processes to correct model mismatch, we converge to a model that matches the actual vehicle dynamics closely. The GP models for error correction are trained on sensor measurements that can be obtained by driving the vehicle around with a model-free controller (like pure pursuit) or even manual control on an arbitrary track, see Section 4.1-4.2. We demonstrate the efficacy of our approach through the design of a motion planner (trajectory generator) and MPC for tracking pre-computed racing lines using this corrected model in Section 4.3. We show that the performance is further enhanced by updating the GP models with data generated by MPC in Section 4.4. Our learning procedure is essential to reducing the cost of system identification and thus enables aggressive controller design. Source code for all experiments and models is available at <https://github.com/jainachin/bayesrace>.

2 Vehicle models

Among many choices for the models of vehicle dynamics, the most widely used are kinematic and dynamic bicycle models, see expressions for a rear-wheel drive in Table 1 and details in [12, 13].

Notation. We use the following notation throughout the paper. *States, inputs, and forces:* x, y are the coordinates in an inertial frame, ψ is the inertial heading, v and a are speed and acceleration in the inertial frame, v_x, v_y are velocities in the body frame, ω is the angular velocity, δ is the steering angle, $\Delta\delta$ is the change in the steering angle, $F_{r,x}$ is the longitudinal force in the body frame, $F_{f,y}$ and $F_{r,y}$ are the lateral forces in the body frame with subscripts f and r denoting front and rear wheels, respectively, α_f and α_r are the corresponding slip angles. *Vehicle model parameters:* m denotes the mass, I_z the moment of inertia about the vertical axis passing through the center of gravity, l_f and l_r the distance of the center of gravity from the front and the rear wheels in the longitudinal direction. $B_f, B_r, C_f, C_r, D_f,$ and D_r are track specific parameters for the tire force curves.

Kinematic model is preferred in some applications [14, 15] for its simplicity as it requires only two tuning parameters, namely lengths l_f and l_r , which can be physically measured. The kinematic model ignores the effect of tire slip and thus does not reflect actual dynamics at high-speed cornering. Therefore, it is considered unsuitable for model-based control in autonomous racing.

Dynamic model, on the other hand, is more complex and painful to tune as it requires several tests to identify tire, drivetrain, and friction parameters. The lateral forces are typically modeled using a Pacejka tire model, see Table 1 and [16]. A complete procedure of system identification is available in [1]. When well-tuned, the dynamic model is considered suitable for autonomous racing in the MPC framework [5, 6, 7, 17]. However, the model complexity makes the tuning procedure

Table 1: Different vehicle models.

VEHICLE DYNAMICS		
Kinematic	Dynamic	Extended kinematic
$\dot{x} = v \cos(\psi + \beta)$	$\dot{x} = v_x \cos \psi - v_y \sin \psi$	$\dot{x} = v_x \cos \psi - v_y \sin \psi$
$\dot{y} = v \sin(\psi + \beta)$	$\dot{y} = v_x \sin \psi + v_y \cos \psi$	$\dot{y} = v_x \sin \psi + v_y \cos \psi$
$\dot{\psi} = \frac{v}{l_r} \sin \beta$	$\dot{\psi} = \omega$	$\dot{\psi} = \omega$
$\dot{v} = a$	$\dot{v}_x = \frac{1}{m} (F_{r,x} - F_{f,y} \sin \delta + m v_y \omega)$	$\dot{v}_x = \frac{1}{m} (F_{r,x})$
$\dot{\delta} = \Delta \delta$	$\dot{v}_y = \frac{1}{m} (F_{r,y} + F_{f,y} \cos \delta - m v_x \omega)$	$\dot{v}_y = \frac{l_r}{l_f + l_r} (\dot{\delta} v_x + \delta \dot{v}_x)$
$\beta = \tan^{-1} \left(\frac{l_r}{l_f + l_r} \tan \delta \right)$	$\dot{\omega} = \frac{1}{I_z} (F_{f,y} l_f \cos \delta - F_{r,y} l_r)$	$\dot{\omega} = \frac{1}{l_f + l_r} (\dot{\delta} v_x + \delta \dot{v}_x)$
	$\dot{\delta} = \Delta \delta$	$\dot{\delta} = \Delta \delta$
PACEJKA TIRE MODEL		
$F_{f,y} = D_f \sin(C_f \arctan(B_f \alpha_f)), \quad \alpha_f = \delta - \arctan\left(\frac{\omega l_f + v_y}{v_x}\right)$ $F_{r,y} = D_r \sin(C_r \arctan(B_r \alpha_r)), \quad \alpha_r = \arctan\left(\frac{\omega l_r - v_y}{v_x}\right)$		

time prohibitive, especially when the tire slip curves must be re-calibrated for a new racing surface, which is indeed common for autonomous racing competitions.

Extended kinematic model. The essential difference between the kinematic and dynamic models is that three states, v_x , v_y , and ω , are not defined in the former. Thus, to easily measure the discrepancy between real measurements and model predictions, we consider a variant of the kinematic model that has the same states as the dynamic model. We call this extended kinematic (e-kinematic) model, see mathematical representation in Table 1. The advantage of using the e-kinematic model is that it has only three tuning parameters, namely m , l_f , and l_r , all of which can be physically measured. However, unlike the dynamic model which is closer to the real dynamics, the e-kinematic model does not consider tire forces. Thus, using it in MPC in its standard form will result in undesirable errors. Specifically, the evolution of the first three states x , y , and ψ is exactly same in the e-kinematic and the dynamic model; the difference lies only in v_x , v_y , and ω . Our learning procedure presented in Section 4 is based on reducing the mismatch between the e-kinematic model and the real measurements (or estimates) of the states x , y , ψ , v_x , v_y , and ω . The e-kinematic model is used in [17] to approximate the vehicle dynamics at low speeds where the Pacejka model is undefined due to division by v_x .

Comparison. We compare the response of all three models with the same inputs in Figure 1. A constant acceleration ($a = \frac{1}{m} F_{r,x}$) of 1 m/s^2 is applied for 1s starting from zero initial speed while the steering angle is kept constant at 0.2 rad. The vehicle parameters are taken from [5]. The impact of model mismatch is evident while turning even at low speeds as nonlinear lateral tire forces start to dominate. The trajectories diverge with time. The real vehicle dynamics are best represented by the orange curve when the dynamic model is well-tuned.

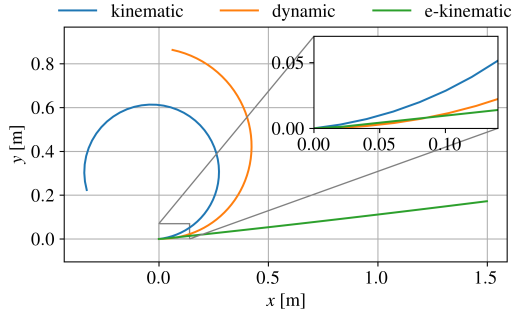


Figure 1: Response of vehicle models under same model inputs. Constant acceleration of 1 m/s^2 is applied for 1s while steering at 0.2 rad.

3 Problem setting

The experiments are performed in simulations on the 1:43 scale autonomous racing platform [5]. See Appendix B for results on the 1:10 platform [18]. The real vehicle dynamics is simulated using the dynamic model f_{dyn} . The model predictive controller uses the e-kinematic model *with* error correction f_{corr} to make real-time decisions for minimizing the lap time. This is graphically illustrated in Figure 2. In Section 4, we show how BAYESRACE learns this error correction function using Gaussian processes. We also compare BAYESRACE to two different scenarios: (1) WORSTCASE when there is no correction for model mismatch, i.e., MPC uses the e-kinematic model f_{kin} in Figure 2, and (2) BESTCASE when MPC has full knowledge of the real dynamics, i.e., MPC uses the dynamic model f_{dyn} in Figure 2.

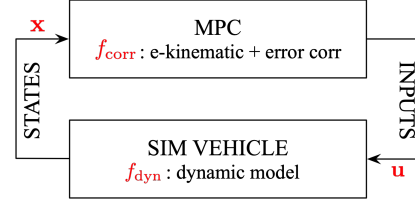


Figure 2: Setup for BAYESRACE.

The vehicle (dynamic model) is powered by a DC electric motor. The longitudinal force is given by

$$F_{r,x} = (C_{m_1} - C_{m_2}v_x)d - C_r - C_d v_x^2, \quad (1)$$

where C_{m_1} and C_{m_2} are the *known* coefficients of the motor model, C_r is the rolling resistance, C_d the drag resistance, and d the pulse width modulation (PWM) duty cycle for the motor. A positive d implies an acceleration and a negative d deceleration. For the e-kinematic model, we further reduce the complexity by ignoring rolling and drag resistance such that

$$F_{r,x} = (C_{m_1} - C_{m_2}v_x)d. \quad (2)$$

Thus, with this definition, the states of both models are defined as $\mathbf{x} := [x, y, \psi, v_x, v_y, \omega, \delta]^T$ and inputs as $\mathbf{u} := [d, \Delta\delta]^T$. We denote the discrete time representation of the e-kinematic model by $\mathbf{x}_{k+1} = f_{\text{kin}}(\mathbf{x}_k, \mathbf{u}_k)$. We assume that the vehicle is equipped with the relevant sensors needed for state estimation, mapping, and localization. For further details, we refer the reader to [17, 19].

4 Learning-based control

We break down our approach into four steps: (1) data capture \rightarrow (2) training of Gaussian process models \rightarrow (3) predictive controller design \rightarrow (4) model update by exploration.

4.1 Gather real data by driving the vehicle with a simple controller

We begin with collecting sensor measurements and actuation data from the vehicle by driving it around using a simple controller. A pure pursuit controller [20] is a popular choice for path tracking and requires little tuning effort; it was reportedly used by three teams in the DARPA Urban Challenge [21]. For a known track, we compute the racing line using [22] and then track it using the pure pursuit controller. The controller gain and look ahead distance are not tuned well to enforce non-aggressive maneuvers. We collect the data sampled every 20 ms in the form of state-action-state pairs, denoted by $\mathcal{D}_{\text{dyn}} = \{\mathbf{x}_k, \mathbf{u}_k, \mathbf{x}_{k+1}\} \forall k \in \{0, 1, \dots, T-1\}$ where T is the length of the trajectory. The racing line and the trajectory taken by the vehicle are shown in Figure 3. As discussed in Section 3 and Figure 2, \mathcal{D}_{dyn} comes from the dynamic model. In practice, one could drive the vehicle on a track using manual controls or use a similar pure pursuit controller to drive it autonomously to collect the real world data.

4.2 Learn Gaussian process models to reduce model mismatch

Training. We use the collected data \mathcal{D}_{dyn} to address the model mismatch between the dynamic and e-kinematic models. Since the parameters of the e-kinematic model f_{kin} are known, we generate a new dataset \mathcal{D}_{kin} that captures its response when excited with the same inputs starting from the same initialization; $\mathcal{D}_{\text{kin}} = \{\mathbf{x}_k, \mathbf{u}_k, f_{\text{kin}}(\mathbf{x}_k, \mathbf{u}_k)\} \forall k \in \{0, 1, \dots, T-1\}$, where $\mathbf{x}_k, \mathbf{u}_k$ come from \mathcal{D}_{dyn} . We define the training data set $\mathcal{D} := \mathcal{D}_{\text{dyn}} \oplus \mathcal{D}_{\text{kin}}$. Our next goal is to learn the model mismatch error in single-step perturbation:

$$\mathbf{e}(\mathbf{x}_k, \mathbf{u}_k) = \mathbf{x}_{k+1} - f_{\text{kin}}(\mathbf{x}_k, \mathbf{u}_k). \quad (3)$$

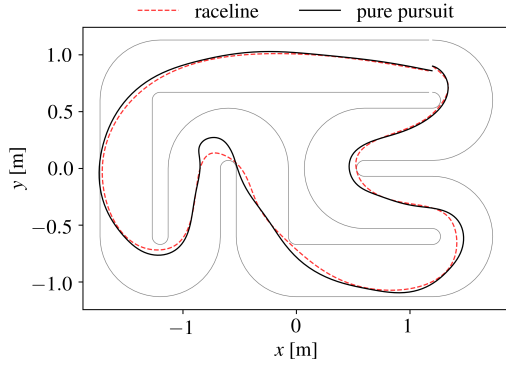


Figure 3: Training: A pure pursuit controller for tracking a racing line is used to generate a *non-aggressive* trajectory. Manual control can also be used instead.

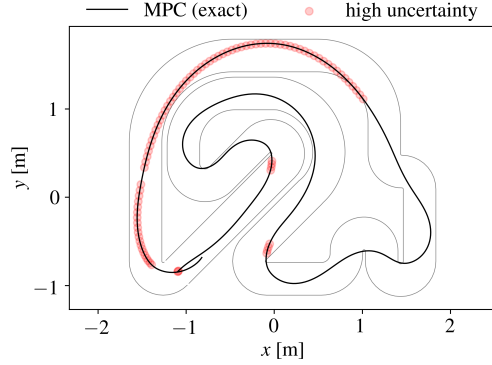


Figure 4: Validation: MPC with full knowledge of the dynamics is used to generate an *aggressive* trajectory. The region with high uncertainty is marked in red.

Note that based on the description in Table 1, \mathbf{x}_{k+1} in \mathcal{D}_{dyn} and $f_{\text{kin}}(\mathbf{x}_k, \mathbf{u}_k)$ in \mathcal{D}_{kin} differ in only three states, namely v_x , v_y , and ω . Thus, error \mathbf{e} is of the form $[0, 0, 0, \star, \star, \star, 0]^T$, where \star denotes nonzero terms. For each state with nonzero error, we learn a Gaussian process model of the form

$$\mathbf{e}_j := \mathcal{GP}(\underbrace{v_x, v_y, \omega, \delta}_{\subset \mathbf{x}_k}, \underbrace{d, \Delta\delta}_{=\mathbf{u}_k}), \quad j \in \{4, 5, 6\}, \quad (4)$$

where j equal to 4, 5, 6 corresponds to the model mismatch in the states v_x , v_y and ω , respectively. More specifically, $\mathbf{e}_4 \sim \mathcal{N}(\mu_{v_x}, \sigma_{v_x})$, $\mathbf{e}_5 \sim \mathcal{N}(\mu_{v_y}, \sigma_{v_y})$ and $\mathbf{e}_6 \sim \mathcal{N}(\mu_{\omega}, \sigma_{\omega})$, where each μ and σ is a function of \mathbf{x}_k and \mathbf{u}_k whose closed-form expressions are known, for more details see [23]. Now the corrected model that is suitable for controller design is related to the e-kinematic model as

$$f_{\text{corr}}(\mathbf{x}_k, \mathbf{u}_k) = f_{\text{kin}}(\mathbf{x}_k, \mathbf{u}_k) + \mathbf{e}(\mathbf{x}_k, \mathbf{u}_k). \quad (5)$$

Validation. We validate the trained GP models (see hyperparameter tuning in Appendix A) on a new track shown in Figure 4. However, this time we drive the car with a more aggressive controller. In practice, we will never know the real vehicle dynamics but for the purpose of testing the quality of the trained models, we consider a trajectory from BESTCASE scenario when an MPC controller is designed to minimize lap time using full knowledge of the dynamics. Thus, this trajectory is simply more aggressive than the one obtained using a pure pursuit controller for training and thus also captures high speed cornering. The mean predictions and 95% confidence intervals for all three erroneous states are shown in Figure 5. The regions with high uncertainty in predictions where $\max\{\sigma_{v_x}, \sigma_{v_y}, \sigma_{\omega}\} > 0.25$ are marked on the track in Figure 4. The GP models have high uncertainty mostly during high-speed cornering and while braking before corners.

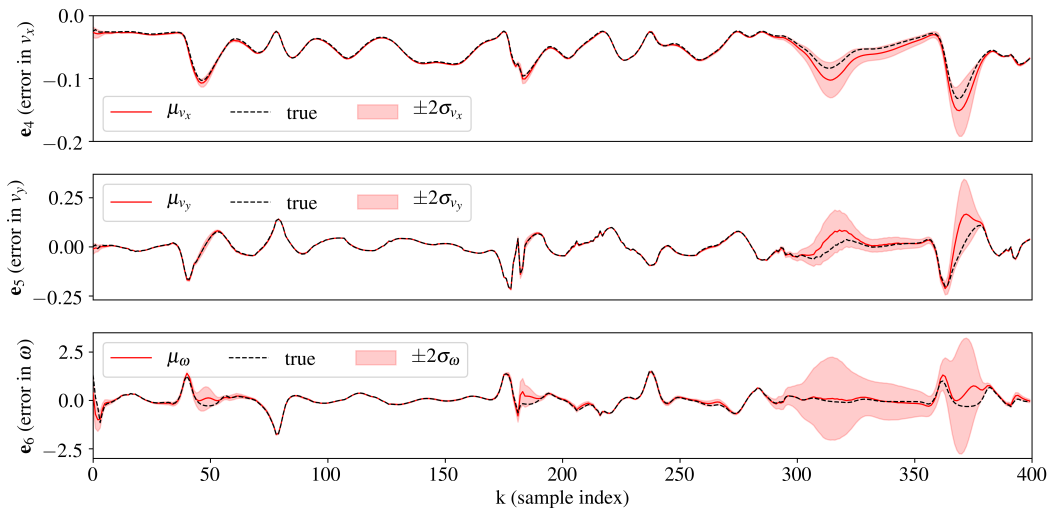


Figure 5: Mean predictions and 95% confidence intervals for errors in v_x , v_y and ω .

4.3 Design nonlinear MPC with corrected extended kinematic model

Controller. Our goal is to design a predictive controller that tracks the racing line using the corrected e-kinematic model f_{corr} . To reduce the computational complexity of the controller, we eliminate stochasticity in (5) by approximating the probability distributions of \mathbf{e}_j by their mean estimates. Thus, the corrected e-kinematic model used in the controller design is given by

$$f_{\text{corr}}(\mathbf{x}_k, \mathbf{u}_k) = f_{\text{kin}}(\mathbf{x}_k, \mathbf{u}_k) + [0, 0, 0, \mu_{v_x}(\mathbf{x}_k, \mathbf{u}_k), \mu_{v_y}(\mathbf{x}_k, \mathbf{u}_k), \mu_{\omega}(\mathbf{x}_k, \mathbf{u}_k), 0]^T. \quad (6)$$

We know the analytical (non-convex) expression of all the μ s from the training step. At any time t , given the current state estimate $\hat{\mathbf{x}}_0(t)$, we solve the following nonlinear program recursively in a receding horizon manner

$$\underset{\mathbf{u}_0, \dots, \mathbf{u}_{N-1}}{\text{minimize}} \quad \sum_{k=1}^N \left\| \begin{matrix} x_k - x_{\text{ref},k} \\ y_k - y_{\text{ref},k} \end{matrix} \right\|_Q + \sum_{k=0}^{N-1} \left\| \begin{matrix} d_k - d_{k-1} \\ \Delta \delta_k \end{matrix} \right\|_R + \|\epsilon_k\|_S \quad (7a)$$

$$\text{subject to} \quad \mathbf{x}_{k+1} = f_{\text{corr}}(\mathbf{x}_k, \mathbf{u}_k), \quad (7b)$$

$$\mathbf{x}_0 = \hat{\mathbf{x}}_0(t), \quad (7c)$$

$$\mathbf{A}_k \begin{bmatrix} x_{k+1} \\ y_{k+1} \end{bmatrix} \leq \mathbf{b}_k + \epsilon_k, \quad (7d)$$

$$d_{\min} \leq d_k \leq d_{\max}, \quad (7e)$$

$$\delta_{\min} \leq \delta_k \leq \delta_{\max}, \quad (7f)$$

$$\Delta \delta_{\min} \leq \Delta \delta_k \leq \Delta \delta_{\max}, \quad (7g)$$

$$\forall k \in \{0, \dots, N-1\}. \quad (7h)$$

Here, the norm $\|z\|_Q := z^T Q z$ and we choose tracking penalty $Q \succ 0$, actuation penalty $R \succ 0$, and slack penalty $S \succ 0$. The reference trajectory $(x_{\text{ref}}, y_{\text{ref}})$ is generated using the motion planner described in the following paragraph. The set of constraints in (7d) come from the track boundary approximated by two hyperplanes for each time step in the horizon. These hyperplanes are parallel to the direction of centerline at the projection of the reference $(x_{\text{ref},k}, y_{\text{ref},k})$ on the centerline. The slack variables ϵ are introduced to prevent infeasibilities. Actuation constraints are defined in (7e)-(7g). The optimization problem is solved every 20 ms using IPOPT [24] with CasADi [25].

Motion planner. The reference trajectory at each time in (7) is based on the racing line computed using Bayesian optimization [22]. This racing line not only provides the path followed around a track $(x_r(\theta), y_r(\theta))$ but also the optimal speed profile $v_r(\theta)$ along the path as a function of the distance traveled along the track θ . For each time step $k \in \{1, \dots, N\}$ we compute

$$\theta_k = \theta_{k-1} + T_s v_r(\theta_{k-1}), \quad (8a)$$

$$x_{\text{ref},k} = x_r(\theta_k), \quad y_{\text{ref},k} = y_r(\theta_k), \quad (8b)$$

where θ_0 is computed at the projection of current position on the racing line and T_s is the sampling time equal to 20 ms. Any other trajectory generator like the lattice planner in [26] can also be used.

Effect of model correction. We show the path followed by the vehicle with BAYESRACE controller (7) in Figure 6. We compare this to WORSTCASE scenario when MPC uses e-kinematic model *without* error correction in Figure 7. In both figures, after every 0.5 s, we also compare the solution of the optimization solver (MPC prediction) in red to the open-loop trajectory obtained by applying the same inputs to the vehicle (in our case, the dynamic model) in green. The higher the deviation between the red and green curves, the higher the model mismatch. If the optimization solver used the exact model for real vehicle dynamics, the only source of discrepancy would be due to discretization. We illustrate how correction with GP models in Figure 6 reduces the model mismatch between the solution returned by the optimization and the open-loop trajectory. As a result, we also observe a reduction in lap times by over 0.5 s. Next, we show a comparison of BAYESRACE controller (7) against BESTCASE scenario case when MPC uses full knowledge of the dynamics and there is no model mismatch in Figure 8. The corresponding set of optimal inputs is shown in Figure 9. Although the inputs show the same pattern, the curves are drifting with time because the model mismatch still persists in f_{corr} .

Figure 6 and 7 show that by error correction with GPs and thus reduction in the model mismatch, we observe the performance is improved to a large extent. However, when compared to the best-case scenario in Figure 8 and 9, we observe there is still scope for improvement. We bridge this gap further by performing a model update in Section 4.4.

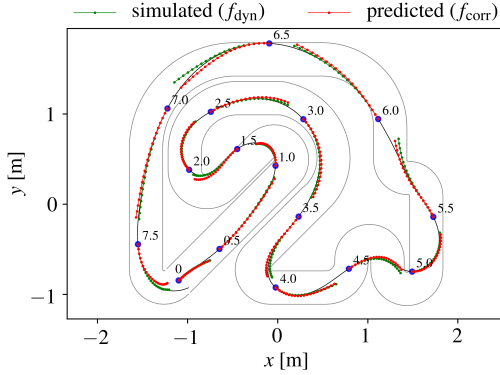


Figure 6: Illustration of model mismatch when GP models are *used* to correct the e-kinematic model.

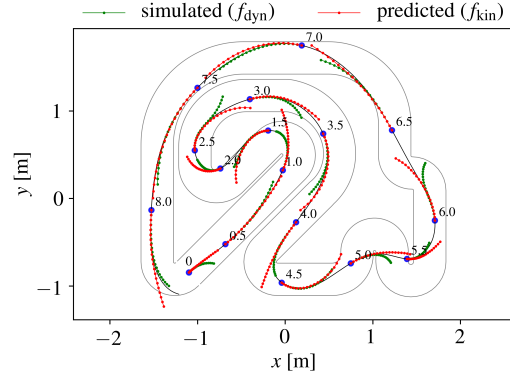


Figure 7: Illustration of model mismatch when GP models are *not* used to correct the e-kinematic model.

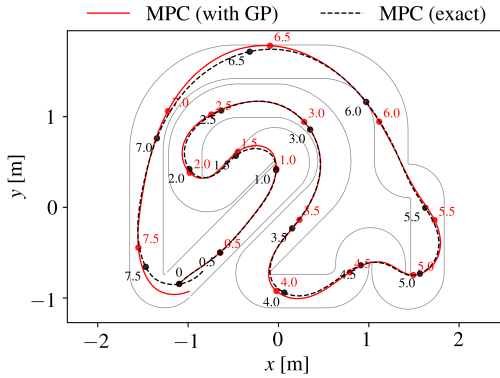


Figure 8: Track position: BAYESRACE controller (7) versus MPC with full knowledge of the dynamics.

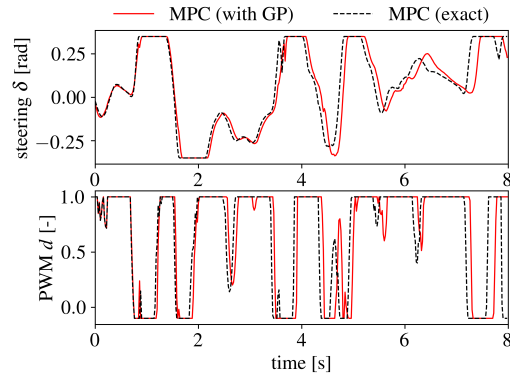


Figure 9: Optimal inputs: BAYESRACE controller (7) versus MPC with full knowledge of the dynamics.

4.4 Update the Gaussian process models after driving the vehicle with MPC

As the final step, we use the data generated by running BAYESRACE controller (7) on the vehicle for one lap to update the GP models (4). Denote these data by $\mathcal{D}_{\text{dyn}}^{\text{mpc}} = \{\mathbf{x}_k, \mathbf{u}_k, \mathbf{x}_{k+1}\} \forall k \in \{0, 1, \dots, T-1\}$ where T is the length of the trajectory. Like in Section 4.2, we also generate a corresponding dataset from the e-kinematic model $\mathcal{D}_{\text{kin}}^{\text{mpc}} = \{\mathbf{x}_k, \mathbf{u}_k, f_{\text{kin}}(\mathbf{x}_k, \mathbf{u}_k)\} \forall k \in \{0, 1, \dots, T-1\}$. Now, to perform the model update, we simply combine the original dataset obtained by running the pure pursuit controller and the new dataset generated by MPC, and then re-train the GP models on $\mathcal{D} = (\mathcal{D}_{\text{dyn}} \cup \mathcal{D}_{\text{dyn}}^{\text{mpc}}) \oplus (\mathcal{D}_{\text{kin}} \cup \mathcal{D}_{\text{kin}}^{\text{mpc}})$. Like in (6), the updated GP models are used to correct the e-kinematic model; we denote this vehicle model by f_{corr}^1 , where superscript denotes number of laps completed with MPC. The controller is updated accordingly to

$$\underset{\mathbf{u}_0, \dots, \mathbf{u}_{N-1}}{\text{minimize}} \quad (7a) \tag{9a}$$

$$\text{subject to} \quad \mathbf{x}_{k+1} = f_{\text{corr}}^1(\mathbf{x}_k, \mathbf{u}_k), \tag{9b}$$

$$(7c) - (7h). \tag{9c}$$

Like in Figure 5, we again use the data generated by BESTCASE MPC with full knowledge of the vehicle dynamics to validate the updated GP models and regenerate the error plots; these are shown in Figure 10. A simple model update after only one lap with MPC suppresses the prediction uncertainty observed in Figure 5 in most regions on the track. However, a little bit of uncertainty persists at the start and the last corner. For practical purposes, f_{corr}^1 represents the real vehicle dynamics closely. We verify this in Figure 11 and 12 by driving a lap with BAYESRACE controller (9) and comparing the solution against BESTCASE MPC with full knowledge of the vehicle dynamics. Note that, to focus only on the effect of model mismatch, we relaxed the penalty on the slack variables for

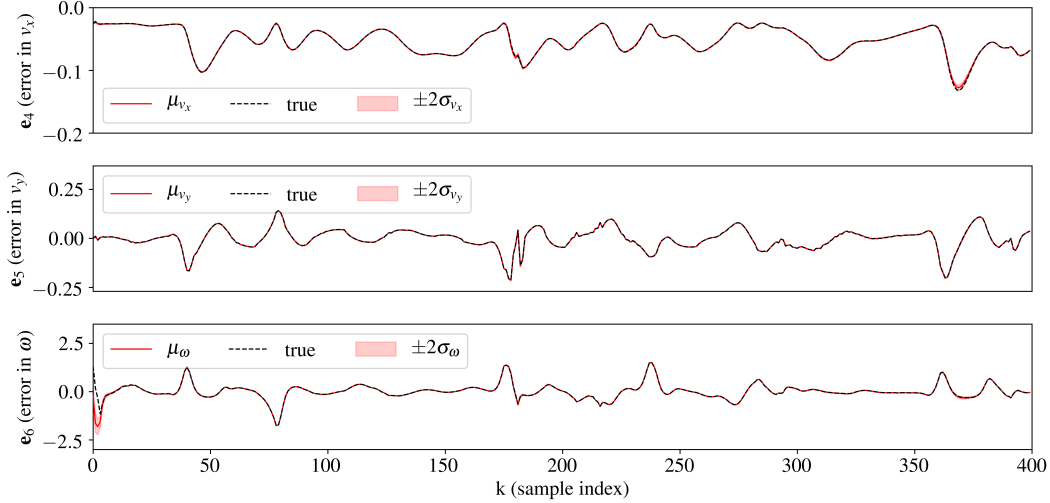


Figure 10: Mean predictions and 95% confidence intervals for errors in v_x , v_y and ω after updating the GPs with one lap of MPC data. Compare this with Figure 5; uncertainty is suppressed in most regions of the track.

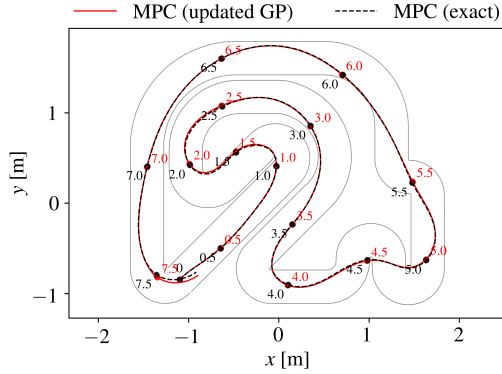


Figure 11: Track position: BAYESRACE controller (9) versus MPC with full knowledge of the vehicle dynamics.

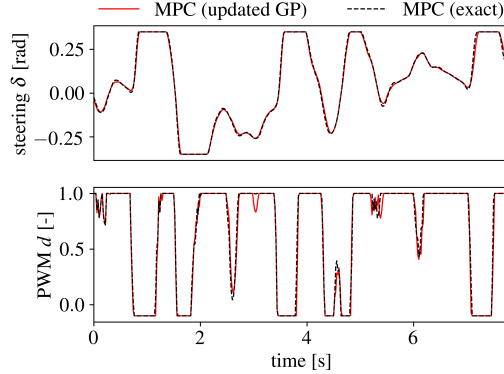


Figure 12: Optimal inputs: BAYESRACE controller (9) versus MPC with full knowledge of the vehicle dynamics.

this comparison (only) to reduce the effect of the boundary constraints on the optimization. Thus, the dashed curve in Figure 8 differs slightly from Figure 11. While we used all of the new data to update the GP models, one could also select specific samples based on prediction of uncertainty on the MPC data $\mathcal{D}_{\text{dyn}}^{\text{mpc}} \oplus \mathcal{D}_{\text{kin}}^{\text{mpc}}$.

5 Conclusions

We present a learning-based planning and control algorithm that significantly reduces the effort required in system identification of an autonomous race car. The real vehicle dynamics are highly nonlinear and difficult to model due to lateral tire forces. Starting with a kinematic model with only three parameters that can be physically measured, our algorithm uses sensor measurements from the vehicle to iteratively correct the (residual) model of the vehicle dynamics. This enables race engineers to design an aggressive model predictive controller without worrying about tuning the vehicle model parameters. We demonstrate the performance and generalization capabilities of our approach using validated simulation of the 1:43 scale autonomous racing platform [5] and the FITENTH autonomous racing platform [27] (Appendix B).

References

- [1] A. Liniger. *Path planning and control for autonomous racing*. PhD thesis, ETH Zurich, 2018.
- [2] M. Bojarski, D. Del Testa, D. Dworakowski, B. Firner, B. Flepp, P. Goyal, L. D. Jackel, M. Monfort, U. Muller, J. Zhang, et al. End to end learning for self-driving cars. *arXiv preprint arXiv:1604.07316*, 2016.
- [3] B. Balaji, S. Mallya, S. Genc, S. Gupta, L. Dirac, V. Khare, G. Roy, T. Sun, Y. Tao, B. Townsend, et al. DeepRacer: Educational autonomous racing platform for experimentation with sim2real reinforcement learning. *arXiv preprint arXiv:1911.01562*, 2019.
- [4] N. R. Kapania and C. J. Gerdes. Path tracking of highly dynamic autonomous vehicle trajectories via iterative learning control. In *Proceedings of the 2015 American Control Conference*, pages 2753–2758. IEEE, 2015.
- [5] A. Liniger, A. Domahidi, and M. Morari. Optimization-based autonomous racing of 1:43 scale RC cars. *Optimal Control Applications and Methods*, 36(5):628–647, 2015.
- [6] U. Rosolia and F. Borrelli. Learning how to autonomously race a car: a predictive control approach. *IEEE Transactions on Control Systems Technology*, 2019.
- [7] L. Hewing, A. Liniger, and M. N. Zeilinger. Cautious NMPC with Gaussian process dynamics for autonomous miniature race cars. In *Proceedings of the 2018 European Control Conference (ECC)*, pages 1341–1348. IEEE, 2018.
- [8] M. Deisenroth and C. E. Rasmussen. PILCO: A model-based and data-efficient approach to policy search. In *Proceedings of the 28th International Conference on machine learning (ICML)*, pages 465–472, 2011.
- [9] A. Kloss, S. Schaal, and J. Bohg. Combining learned and analytical models for predicting action effects from sensory data. *The International Journal of Robotics Research*, 2018.
- [10] A. Ajay, J. Wu, N. Fazeli, M. Bauza, L. P. Kaelbling, J. B. Tenenbaum, and A. Rodriguez. Augmenting physical simulators with stochastic neural networks: Case study of planar pushing and bouncing. In *2018 IEEE/RSJ International Conference on Intelligent Robots and Systems (IROS)*, pages 3066–3073. IEEE, 2018.
- [11] A. Zeng, S. Song, J. Lee, A. Rodriguez, and T. Funkhouser. Tossingbot: Learning to throw arbitrary objects with residual physics. *IEEE Transactions on Robotics*, 2020.
- [12] J. Kong, M. Pfeiffer, G. Schildbach, and F. Borrelli. Kinematic and dynamic vehicle models for autonomous driving control design. In *Proceedings of the 2015 IEEE Intelligent Vehicles Symposium (IV)*, pages 1094–1099, 2015.
- [13] R. Rajamani. *Lateral Vehicle Dynamics*, pages 15–46. Springer US, Boston, MA, 2012. ISBN 978-1-4614-1433-9. doi:10.1007/978-1-4614-1433-9_2.
- [14] S. Thrun, M. Montemerlo, H. Dahlkamp, D. Stavens, A. Aron, J. Diebel, P. Fong, J. Gale, M. Halpenny, G. Hoffmann, et al. Stanley: The robot that won the DARPA Grand Challenge. *Journal of Field Robotics*, 23(9):661–692, 2006.
- [15] Y. Kanayama, Y. Kimura, F. Miyazaki, and T. Noguchi. A stable tracking control method for an autonomous mobile robot. In *Proceedings of the IEEE International Conference on Robotics and Automation*, pages 384–389. IEEE, 1990.
- [16] E. Bakker, L. Nyborg, and H. B. Pacejka. Tyre modelling for use in vehicle dynamics studies. *SAE Transactions*, pages 190–204, 1987.
- [17] J. Kabzan, M. I. Valls, V. Reijgwart, H. F. Hendriks, C. Ehmke, M. Prajapat, A. Bühler, N. Gosala, M. Gupta, R. Sivanesan, et al. AMZ Driverless: The full autonomous racing system. *arXiv preprint arXiv:1905.05150*, 2019.

- [18] M. O’Kelly, H. Zheng, D. Karthik, and R. Mangharam. F1TENTH: An open-source evaluation environment for continuous control and reinforcement learning. In *Post Proceedings of the NeurIPS 2019 Demonstration and Competition Track*, 2020.
- [19] M. I. Valls, H. F. Hendriks, V. J. Reijgwart, F. V. Meier, I. Sa, R. Dubé, A. Gawel, M. Bürki, and R. Siegwart. Design of an autonomous racecar: Perception, state estimation and system integration. In *Proceedings of the 2018 IEEE International Conference on Robotics and Automation (ICRA)*, pages 2048–2055. IEEE, 2018.
- [20] R. C. Coulter. Implementation of the pure pursuit path tracking algorithm. Technical report, Carnegie Mellon University, 1992.
- [21] M. Buehler, K. Iagnemma, and S. Singh. *The DARPA Urban Challenge: Autonomous vehicles in city traffic*, volume 56. Springer, 2009.
- [22] A. Jain and M. Morari. Computing the racing line using Bayesian optimization. In *Proceedings of the 59th IEEE Conference on Decision and Control (CDC)*, 2020.
- [23] C. E. Rasmussen and C. K. Williams. *Gaussian processes for machine learning*, volume 1. MIT press Cambridge, 2006.
- [24] A. Wächter and L. Biegler. IPOPT- an Interior Point OPTimizer, 2009.
- [25] J. A. E. Andersson, J. Gillis, G. Horn, J. B. Rawlings, and M. Diehl. CasADi – A software framework for nonlinear optimization and optimal control. *Mathematical Programming Computation*, 2018.
- [26] T. M. Howard and A. Kelly. Optimal rough terrain trajectory generation for wheeled mobile robots. *International Journal of Robotics Research*, 2007.
- [27] M. O’Kelly, V. Sukhil, H. Abbas, J. Harkins, C. Kao, Y. V. Pant, R. Mangharam, D. Agarwal, M. Behl, P. Burgio, and M. Bertogna. F1/10: An open-source autonomous cyber-physical platform.
- [28] M. Althoff. Commonroad: Vehicle models. *Technische niversität München, Garching*, pages 1–25, 2017.
- [29] A. Sinha, M. O’Kelly, H. Zheng, and R. Mangharam. FormulaZero: Distributionally robust online adaptation via offline population synthesis. In *Proceedings of the International Conference on Machine Learning (ICML)*, 2020.
- [30] M. O’Kelly, H. Zheng, A. Jain, J. Auckley, K. Luong, and R. Mangharam. TunerCar: A super-optimization toolchain for autonomous racing. In *Proceedings of the International Conference on Robotics and Automation (ICRA)*, 2020.
- [31] A. Bulsara, A. Raman, S. Kamarajugadda, M. Schmid, and V. N. Krovi. Obstacle avoidance using model predictive control: An implementation and validation study using scaled vehicles. *SAE Technical Paper*, 2020.
- [32] R. Ivanov, T. J. Carpenter, J. Weimer, R. Alur, G. J. Pappas, and I. Lee. Case study: verifying the safety of an autonomous racing car with a neural network controller. In *Proceedings of the 23rd International Conference on Hybrid Systems: Computation and Control*, pages 1–7, 2020.
- [33] O. Klimov. Carracing-v0. 2016. URL <https://gym.openai.com/envs/CarRacing-v0>.
- [34] C. Walsh and S. Karaman. CDDT: Fast approximate 2D ray casting for accelerated localization. *arXiv preprint arXiv:1705.01167*, 2017. URL <http://arxiv.org/abs/1705.01167>.
- [35] A. Domahidi and J. Jerez. Forces professional. <http://embotech.com/FORCES-Pro>, 2014. Accessed: 2020-02-07.

A Gaussian process modeling

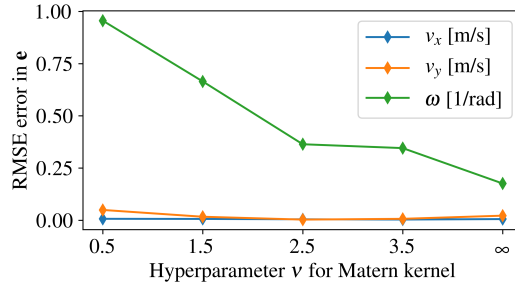


Figure 13: Tuning of smoothness parameter in the Matérn kernel used to model Gaussian processes (4).

A Gaussian process (GP) is a collection of random variables, any finite number of which have a joint Gaussian distribution. Consider noisy observations y of an underlying function $f : \mathbb{R}^n \mapsto \mathbb{R}$ through a Gaussian noise model: $y = f(x) + \mathcal{N}(0, \sigma_n^2)$, $x \in \mathbb{R}^n$. A GP of y is fully specified by its mean function $\mu(x)$ and covariance function $k(x, x')$,

$$\begin{aligned} \mu(x; \theta) &= \mathbb{E}[f(x)] \\ k(x, x'; \theta) &= \mathbb{E}[(f(x) - \mu(x))(f(x') - \mu(x')))] + \sigma_n^2 \delta(x, x') \end{aligned} \quad (10)$$

where $\delta(x, x')$ is the Kronecker delta function. The hyperparameter vector θ parameterizes the mean and covariance functions. We denote this GP by $y \sim \mathcal{GP}(x; \theta)$. For more details, see [23].

In Section 4.2, we chose GPs for modeling because they work well for smooth function approximation and small datasets. Specifically, we learn three GP models to predict model mismatch:

$$e_j := \mathcal{GP}(\underbrace{v_x, v_y, \omega}_{\mathbf{C}\mathbf{x}_k}, \underbrace{\delta, d, \Delta\delta}_{=\mathbf{u}_k}), \quad j \in \{4, 5, 6\}, \quad (11)$$

where j equal to 4, 5, 6 corresponds to the model mismatch in the states v_x , v_y and ω , respectively. We use a constant mean function and the Matérn kernel for all three models. We show the tuning of the smoothness parameter in the Matérn kernel in Figure 13. We chose $\nu \rightarrow \infty$; the Matérn kernel is equivalent to the RBF kernel in this limit. For experiments on the F1TENTH platform in Appendix B, a finite value of ν provided better results.

B Experiments on F1TENTH platform

We test the generalization of our approach via the use of a second experimentally validated simulator.

F1TENTH Platform. The F1TENTH platform [27] includes a validated simulator which has been previously used to successfully transfer simulation-based raceline-optimization to the real world. The simulator utilizes the single-track bicycle model (see [28], equation (9) on page 6). The applicability of our method, given successful experiments on the F1TENTH simulator, is supported by numerous results which use the F1TENTH simulator to design control policies prior to deployment on real robots [29, 30, 18, 31, 32].

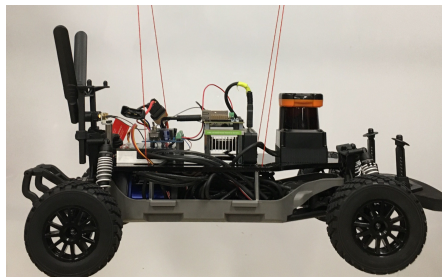


Figure 14: Extensive system identification has been performed on a F1TENTH vehicle.

Experiment design. We adapt a random track generator based on the OpenAI gym car-racing environment [33] for use in the F1TENTH simulator. We generate four new tracks, one for training the vehicle model, and three for validation of the learned model. We conduct experiments as though we are using the real vehicle: (1) implementing a simple controller to excite the vehicle states, (2) logging data, (3) training a GP-based dynamics correction model, (4) computing the racing line, (5) then executing the MPC, and (6) measuring both the lap time and quality of the GP models’ predictions. To move from the 1:43 scale simulator in Section 4 to F1TENTH, the only change made was the tuning of the smoothness hyperparameter (a scaler) of each Matèrn GP kernel; see Appendix A. The MPC controller was *not* tuned again. The benefit of using GPs for model correction is shown in Figure 15 and 16. The lap time improves by over 2.5 seconds.

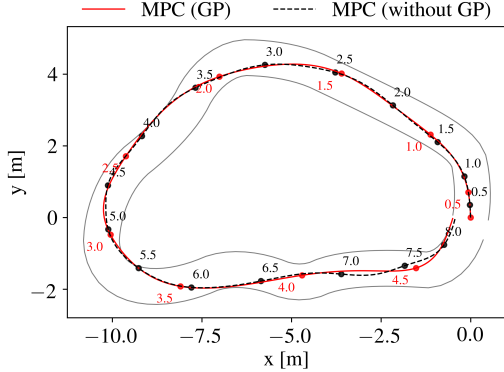


Figure 15: Track position: BAYESRACE controller versus MPC with no model correction.

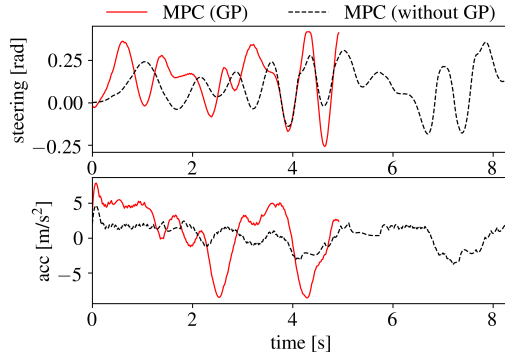


Figure 16: Optimal inputs: BAYESRACE controller versus MPC with no model correction.

Reality gap. As noted in Section 3, our scientific objective is not to design better mechanisms for localization or odometry measurement. Rather we assume that the vehicle has sufficient sensors to measure the states of interest necessary to train the GP model, *c.f.* [17, 19]. The F1TENTH vehicle includes an on-board LIDAR and motor controller which can estimate the wheel odometry. Fusing these measurements with the control inputs via a particle filter enables accurate collection of all relevant data [34]. The other aspect of this work which would need to be adapted for deployment is the execution time of MPC controller. On a 2.9 GHz Dual-Core Intel Core i5 MacOS we measure 0.26 ± 0.1 seconds. While it may be feasible for the vehicle to complete a lap despite the controller latency, an order of magnitude better performance is possible if a commercial solver such as FORCES PRO [35] is utilized. In this submission, we provide code which instead uses the slower but more permissively licensed IPOPT solver [24] with CasADi [25].